Journal of Power Sources 194 (2009) 1094–1098

Contents lists available at ScienceDirect

Journal of Power Sources

journal homepage: www.elsevier.com/locate/jpowsour

Short communication

Fast sol–gel synthesis of $LiFePO_4/C$ for high power lithium-ion batteries for hybrid electric vehicle application

Sabina Beninati, Libero Damen, Marina Mastragostino*

University of Bologna, Department of Metal Science, Electrochemistry and Chemical Techniques, Via San Donato 15, 40127 Bologna, Italy

ARTICLE INFO

Article history:
Received 27 April 2009
Received in revised form 4 June 2009
Accepted 12 June 2009
Available online 21 June 2009

Keywords:
$LiFePO_4/C$
Power-assist HEV
Fast sol–gel synthesis

ABSTRACT

$LiFePO_4/C$ of high purity grade was successfully synthesized by microwave accelerated sol–gel synthesis and showed excellent electrochemical performance in terms of specific capacity and stability. This cathode material was characterized in battery configuration with a graphite counter electrode by USABC–DOE tests for power-assist hybrid electric vehicle. It yielded a non-conventional Ragone plot that represents complexity of battery functioning in power-assist HEV and shows that the pulse power capability and available energy of such a battery surpasses the DOE goal for such an application.

1. Introduction

Carbon-coated lithium iron phosphate ($LiFePO_4/C$) is the most popular cathode materials for safe, high power lithium-ion batteries in large format modules that are required for power-assist in full hybrid electric vehicles (HEVs). The advantages of this non-toxic insertion material featuring a theoretical specific capacity of 170 mAh g^{-1} are lithium insertion/extraction at less positive potentials than those of transition metal (Ni, Co and Mn) oxides and greater thermal stability against oxygen release, which makes it safer and more tolerant to abusive conditions. The carbon coating of the $LiFePO_4$ particles enhances its intrinsically low electronic conductivity, and several synthesis routes, including solid-state reactions, hydrothermal syntheses, carbothermal reductions, sol–gel syntheses and microwave processing have been pursued to prepare nanostructured $LiFePO_4/C$, as recently reviewed in ref. [1]. Critical to the success of the electrochemical performance of $LiFePO_4/C$ is its preparation method, which in turn controls morphology, particle size and cation order. Even the purity grade of synthesis precursors is critical because impurities can block one-dimensional channels for lithium motion, and an exact stoichiometry of the lithium iron phosphate without excess or deficiency of lithium is of great importance to approach the theoretical capacity [2].

We report the results of electrochemical tests on $LiFePO_4/C$ prepared by sol–gel synthesis starting from home-made Fe(III)-citrate with accelerated gel formation by microwave (MW) processing. The results include electrode material characterization in cell *vs.* Li and in battery configuration, the latter performed on the basis of the United States Advanced Battery consortium (USABC) and Department of Energy (DOE) FreedomCAR protocol to simulate the dynamic functioning of the battery in power-assist full HEVs [3,4].

2. Experimental

The chemicals for $LiFePO_4/C$ synthesis were Fe(III)-citrate, $C_6H_5FeO_7$ and commercial H_3PO_4 and Li_3PO_4 from Sigma–Aldrich. The $C_6H_5FeO_7$ was prepared after ref. [5] by adding a citric acid (Fluka) solution to one of $Fe(OH)_3$ and heating at 90 °C for 2 h under stirring and then separating the product by precipitation with acetone. The purity grade of the $C_6H_5FeO_7$ was 96.5% as estimated by spectrophotometric measurements as follows: a few mg of Fe(III)-citrate were dissolved in 0.2 M HNO_3 and mixed with a solution of potassium thiocyanate (Sigma–Aldrich) to form a complex with maximum absorbance at 480 nm; the molar absorption coefficient at this wavelength as evaluated by a standard solution of Fe(III)-nitrate in 0.5 M HNO_3 from Merck was $\varepsilon = 9.73 \times 10^3$ l mol^{-1} cm^{-1}.

The MW oven (2.45 GHz) was a single-mode CEM Discover scientific oven [6]. The XRD analysis was performed by a Philips PW1710 diffractometer, a Cu Kα (λ = 1.5406 Å) radiation source and Ni filter with continuous acquisition in 10–80° 2θ range, 0.05° 2θ s^{-1} scan rate. The TGA was carried out by Mettler Toledo TGA/SDTA A851 from room temperature (RT) to 700 °C (heating rate 5 °C min^{-1}) in O_2 flux. The potentiometric titration analyses were performed by a 794 Basic Titrino (Metrohom).

Electrochemical characterization of $LiFePO_4/C$ was carried out on composite electrodes prepared by lamination on carbon-coated

* Corresponding author. Tel.: +39 051 2099798; fax: +39 051 2099365.
E-mail address: marina.mastragostino@unibo.it (M. Mastragostino).

0378-7753/$ – see front matter © 2009 Elsevier B.V. All rights reserved.
doi:10.1016/j.jpowsour.2009.06.035

aluminum grid (Lamart) of a paste obtained by mixing 80 wt.% $LiFePO_4$/C, 15 wt.% carbon conducting additive (SuperP, MMM Carbon Co.) and 5 wt.% polytetrafluoroethylene (Du Pont, 60 wt.% water dispersion) binder in a small amount of ethanol; the electrodes were dried at 80 °C under vacuum over night before use. The geometric electrode area was 0.61 cm^2 and the composite mass loading was in the range 5–7 mg cm^{-2} of geometric area. "T-type" electrochemical cells with Li reference electrode were used for $LiFePO_4$/C electrode characterization both in cell *vs*. Li and in battery configuration. While Li in excess was the counter for the former, a graphite electrode with balanced capacity was used for the battery. The graphite electrodes were prepared by lamination on copper grid (Lamart) of a paste obtained by mixing 88 wt.%. Timrex KS-15 (Timcal) graphite (dried at 200 °C under vacuum over night), 5 wt.% carbon SuperP and 7 wt.% polytetrafluoroethylene in a small amount of ethanol, and the electrodes were further dried over night at 100 °C under vacuum before battery assembly. A dried and degassed glass separator (Whatman GF/D 400-μm thick) was used after soaking in the same electrolyte of the electrochemical cell ethylene carbonate (EC):dimethylcarbonate (DMC) 2:1–1 M $LiPF_6$ (Merck LP31) or EC: DMC 1:1–1 M $LiPF_6$ (Ferro Corp.). Cell assembly and sealing were performed in an argon atmosphere MBraun Labmaster 130 dry box (H_2O and O_2 < 1 ppm) and the electrochemical tests were performed by PerkinElmer VMP multichannel potentiostat.

3. Results and discussion

3.1. Synthesis and characterization

The precursors of sol–gel synthesis of carbon-coated lithium iron phosphate were Fe(III)-citrate, H_3PO_4 and Li_3PO_4, dissolved in water in exact stoichiometric molar ratio (Li:Fe:P = 1:1:1) as in ref. [7] and without any additional source of carbon than the citrate anion. After precursor dissolution in water, we accelerated the gel formation step by MW processing that in a few minutes, instead of the several hours needed in a conventional sol–gel synthesis, provided an efficient water removal. As an example, 50 ml of solution containing 2 g of Fe(III)-citrate and stoichiometric amounts of H_3PO_4 and Li_3PO_4 was completely dried after 12 min of MW processing under stirring in the CEM Discover oven set at the 300 W maximum power; as the temperature started to increases rapidly above 100 °C, the MW radiation automatically stopped. The dry gel was ground with a mortar and pestle and then pyrolyzed in furnace under reductive atmosphere (5% hydrogen in argon, 300 ml min^{-1}) for 1 h at 700 °C (heating rate 20 °C min^{-1}). The product, a black powder, was further ground in a mortar and chemically and structurally characterized before electrode preparation. Fig. 1 shows the X-ray pattern of the $LiFePO_4$/C powder: the peaks are all related to $LiFePO_4$, thereby demonstrating the efficacy of the fast synthesis procedure, and the crystallite size of the $LiFePO_4$ was 45 nm, as evaluated by Scherrer's equation from the 200 peak of XRD.

To test the effectiveness of synthesis for yielding $LiFePO_4$/C free from Fe(III) we performed the following analyses. We evaluated the amount of Fe(II) in the synthesized powder by potentiometric titration with potassium dichromate: ca. 50 mg of powder were dissolved in 10 ml of oxygen free HCl/H_2O 1:1 and titrated under Ar. The amount of Fe(II) was then compared to that of total iron, estimated by spectrophotometric measurements as for the $C_6H_5FeO_7$ analysis, after $LiFePO_4$/C dissolution in hot concentrated HNO_3. Given that the amount of bivalent iron and total iron was the same (33.0 wt.%), we concluded that the $LiFePO_4$/C did not contain Fe(III) impurities.

The content of carbon in $LiFePO_4$/C was evaluated from the difference between the amount of $LiFePO_4$ in the powder, as estimated by titration analysis, and the total weight of the powder, assuming

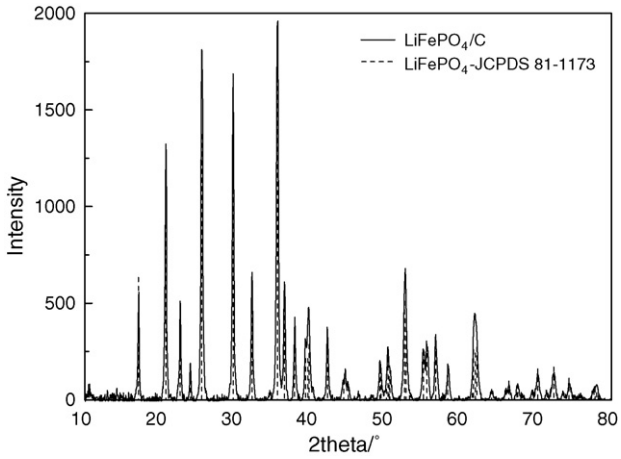

Fig. 1. XRD pattern of $LiFePO_4$/C powder and standard $LiFePO_4$.

that the only components of the synthesized product were $LiFePO_4$ and carbon. We found the amount of carbon to be 6.8% (w/w), which was confirmed by TGA analysis performed by heating $LiFePO_4$/C powder samples in O_2 flux from RT up to 700 °C. The oxygen burns off the carbon and causes the complete oxidation of $LiFePO_4$ to $Li_3Fe_2(PO_4)_3$ and Fe_2O_3 [8].

3.2. Electrochemical tests

The electrochemical characterization of the $LiFePO_4$/C composite electrodes was first carried out in cell configuration *vs*. Li by conventional deep galvanostatic charge–discharge cycles; the electrode rate and cyclability performance are shown in Figs. 2 and 3. Fig. 2 shows deep discharge curves at different C-rate from 0.1 C to 20 C, at 30 °C of fully charged electrodes. At the lowest current density the delivered capacity is 150 mAh g^{-1} and at 20 C it approaches 80 mAh g^{-1}, the latter being one of the best capacity values delivered at such a high C-rate by nanostructured carbon-coated lithium iron phosphate [9–11]. Fig. 3 displays the reversible capacity of these composite electrodes over 50 deep galvanostatic cycles at 0.1 C and over 600 cycles at 1 C-rate, at 30°, thereby demonstrating the high cycling stability of these $LiFePO_4$/C composite electrodes.

To further investigate the $LiFePO_4$/C-rate performance, sequences of 10 s discharge–charge galvanostatic pulses were carried out at different C-rates with 5 C increment on electrodes at

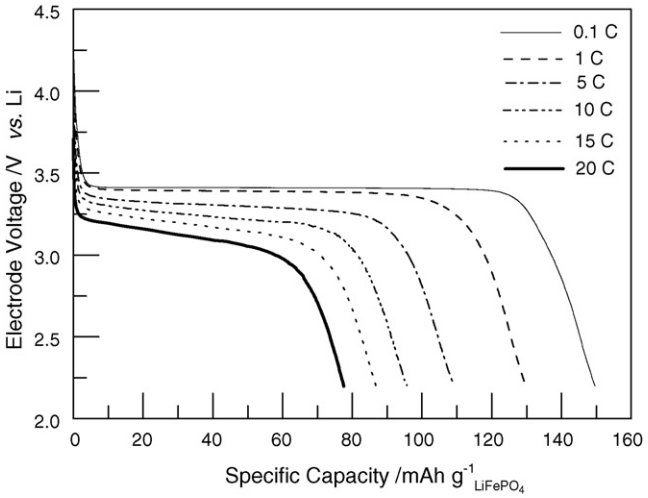

Fig. 2. Discharge profiles of synthesized $LiFePO_4$/C at different C-rates. Cut-off 4.3–2.2 V *vs*. Li.

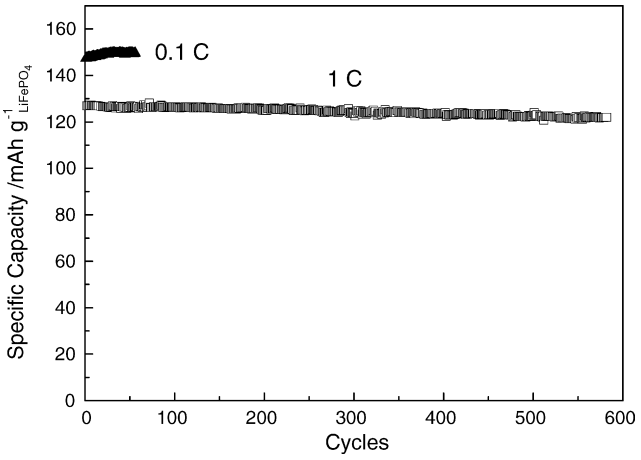

Fig. 3. Specific discharge capacity over cycle number of the $LiFePO_4$/C at 0.1 and 1 C. Cut-off 4.3–2.2 V *vs.* Li.

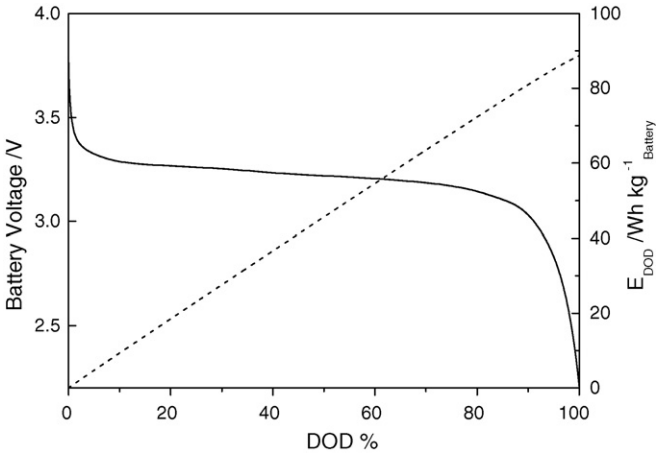

Fig. 5. Static capacity test (SCT) at 1 C-rate and 30 °C on the $LiFePO_4$/C-graphite battery. Dashed line is the relationship between cumulative energy and DOD.

50% depth of discharge (DOD); each pulse was followed by 300 s in open circuit voltage (OCV). Fig. 4 shows, as an example, the voltage profile *vs.* Li of these sequences from 5 C to 45 C for an electrode with $LiFePO_4$/C mass loading of 6.44 mg cm^{-2}. The figure indicates that even at the highest C-rate the discharge–charge pulse maintains the electrode potential inside the cut-off of 4.3–2.2 V *vs.* Li. The maximum specific power calculated from the delivered energy in the 10 s discharge pulse at 45 C was 20.1 kW per kg of $LiFePO_4$/C, a result demonstrating the high pulse rate performance of this cathode material prepared by fast sol–gel procedure.

We then characterized the $LiFePO_4$/C electrodes in battery configuration by USABC–DOE benchmark tests to simulate dynamic battery functioning in power-assist full HEV, where the battery is used during acceleration for a short time and kept within a DOD range (never approaching the fully charged or fully discharged state) by the regenerative braking or the engine. As reported in the "FreedomCAR battery Test Manual for Power-Assist Hybrid Electric Vehicle"[3], the USABC–DOE tests include a static capacity test (SCT) at 1 C discharge rate and a hybrid pulse power characterization (HPPC) tests at 30 °C, which provide the battery dynamic-power capability over usable charge and voltage ranges. A lower voltage limit (V_{MIN}) for battery discharge of 55% of the maximum (V_{MAX}) is recommended as well as HPPC tests at low and at high current. Each test incorporates both discharge and regenerative pulses: the battery is first pulse discharged for 10 s at the stated C-rate, then allowed to relax to the OCV for 40 s, and finally charged for 10 s with a regenerative pulse at 75% current of the discharge pulse. This sequence is repeated, from 10% to 90% DOD, with 10% increment through discharge steps at 1 C-rate, each followed by a 1-h rest period before applying the next sequence. The HPPC test begins with a fully 1-C charged battery after 1 h OCV rest and ends before 90% DOD if the battery voltage exceeds the V_{MAX} in regenerative or V_{MIN} in discharge pulse. The results of the SCT and HPPC tests are used to plot the available energy *vs.* pulse power capability and evaluate whether the battery matches the target for power-assist full HEV.

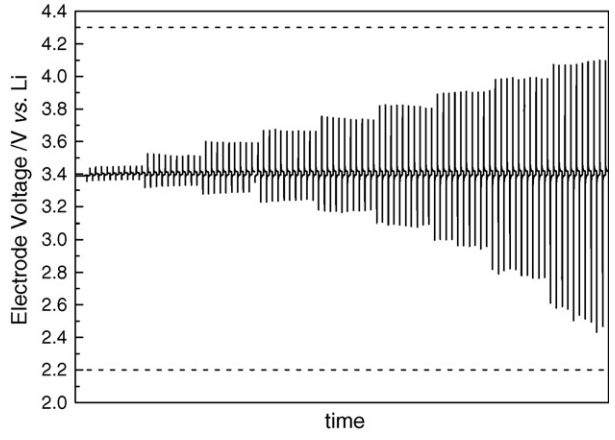

Fig. 4. Voltage profiles of sequences of 10 s discharge–charge galvanostatic pulses carried out at 5–40 C, 5 C increment. Cut-off potentials are also indicated (dashed line).

The FreedomCAR tests of the lithium-ion battery we assembled with $LiFePO_4$/C cathode and graphite anode were performed by setting the V_{MAX} at 4.0 V and the V_{MIN} at 2.2 V; the low-current HPPC test was carried out at the protocol discharge rate of 5 C and the high-current's at 10 C. All the specific parameters evaluated by these tests refer to a total battery mass ($w_{battery}$) which is twice the composite electrode mass of both electrodes ($w_{c.m.}$). Fig. 5 shows, according to SCT test, the plots of the battery discharge voltage and of the specific cumulative energy removed during discharge (E_{DOD}) *vs.* DOD at 1 C-rate and 30 °C.

Fig. 6a displays the voltage profile of the battery (solid line) and of each electrode *vs.* Li reference electrode (dashed and dotted lines) along the sequence of the low-current HPPC test at different DOD from 10% to 90%, separated by 10% DOD. The plots also display the profiles during the full battery charge (1 C galvanostatic/1 h potentiostatic) and the equilibration time (1 h OCV rest) before the beginning of the test. They further display the repetition of the 10% DOD discharge at 1 C-rate followed by 1 h OCV rest and the HPPC test at each DOD. These HPPC tests include pulse discharge at 5.81 mA cm^{-2} (for 0.61 cm^2 electrode area, i_{disc} = 3.54 mA) for 10 s, 40 s rest to relax to OCV, and regenerative pulse for 10 s at 2.60 mA. Fig. 6b shows the magnification of the HPPC voltage profile at 10% DOD, as an example, to mark the values V_0 and V_2, which are the battery potentials just before the discharge and regenerative pulses, respectively, and the values V_1 and V_3, which are the potentials at the end of these pulses. These potential values were used to calculate at different DOD along the FreedomCAR protocol the 10 s discharge and regenerative pulse resistance, R_{disc} and R_{reg}, respectively, as in Eqs. (1) and (2):

$$R_{disc} = \frac{(V_0 - V_1)}{i_{disc}} \quad (1)$$

$$R_{reg} = \frac{(V_3 - V_2)}{i_{reg}} \quad (2)$$

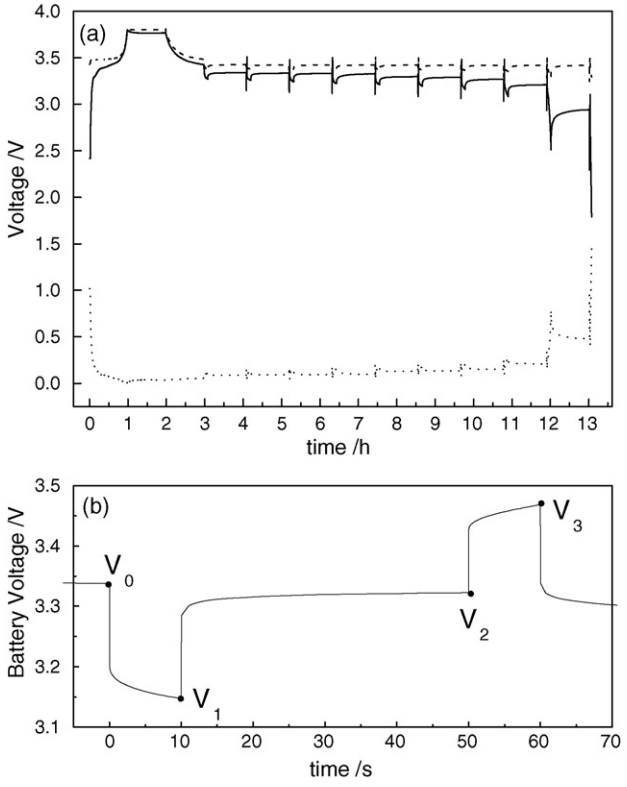

Fig. 6. (a) Voltage profiles of the low-current HPPC performed on the $LiFePO_4$/C-graphite. (—) Battery voltage, (—) cathode and (···) anode voltages; (b) magnification of one voltage impulse of the battery.

The specific discharge (P_{dis}) and regenerative (P_{reg}) pulse power capability at each DOD were then evaluated, as in Eqs. (3) and (4):

$$P_{disc} = \frac{2.2(OCV_{disc} - 2.2)}{(R_{disc}\, w_{module})} \quad (3)$$

$$P_{reg} = \frac{4.0(4.0 - OCV_{regen})}{(R_{reg}\, w_{module})}, \quad (4)$$

where OCV_{disc} is the measured open circuit voltage at the end of each HPPC rest-period and OCV_{regen} the interpolated value through the measured data. Similarly, Fig. 7 displays the voltage profiles along the sequence of the high-current (10 C) HPPC test from 10% DOD to 70%, with discharge pulse current of 7.09 mA and regenerative of 5.31 mA.

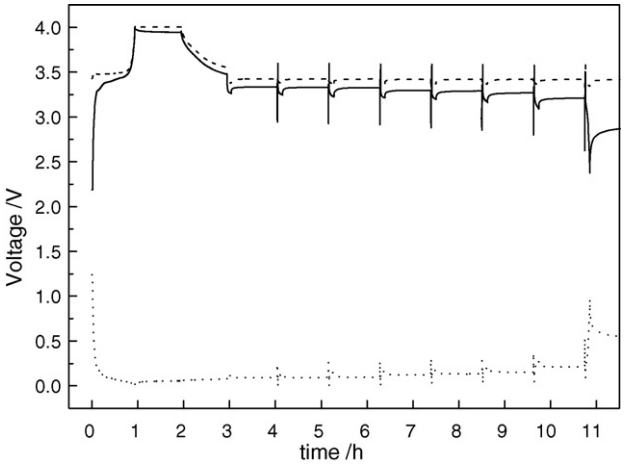

Fig. 7. Voltage profile of the high-current HPPC performed on the LiFePO4/C-graphite battery. (—) Battery voltage, (—) cathode and (···) anode voltages.

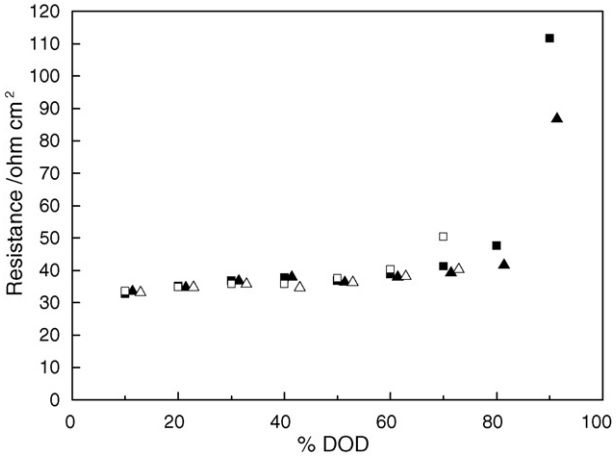

Fig. 8. Pulse resistances *vs.* %DOD: (■) and (▲) are R_{dis} and R_{regen} calculated from the low-current HPPC test; (□) and (△) are R_{dis} and R_{regen} calculated from the high-current one.

Fig. 8 shows the resistance values, R_{disc} and R_{reg}, *vs.* DOD and Fig. 9 the corresponding pulse power capability values, P_{disc} and P_{reg}, calculated from low-current HPPC test up to 90% DOD and high-current up to 70%. Fig. 9 also displays the minimum pulse power goal stated by DOE FreedomCAR for power-assist HEV (dashed line) and shows that all the pulse power data go beyond this goal, the

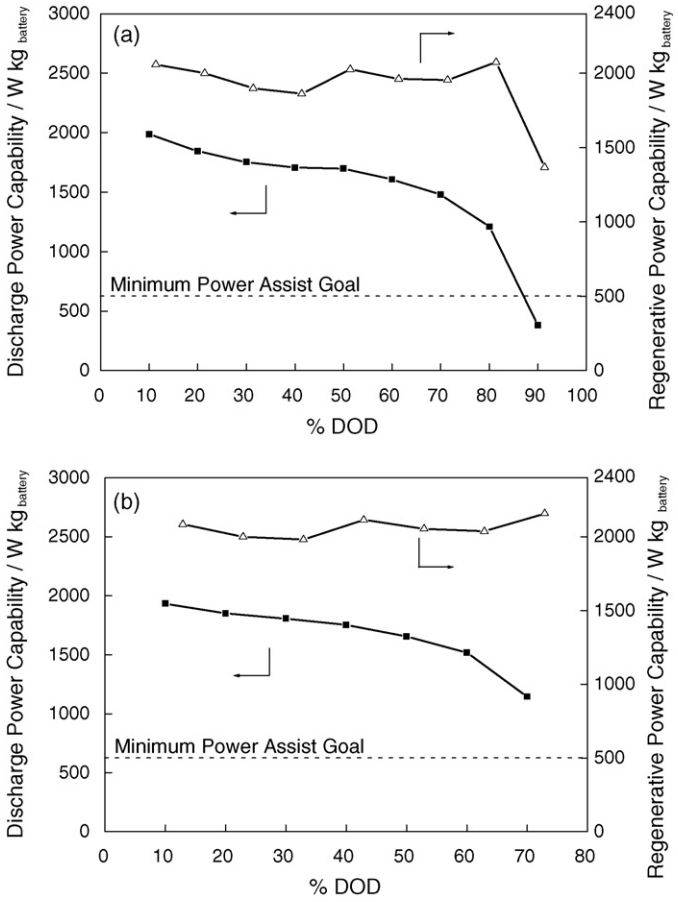

Fig. 9. Discharge and regenerative pulse-power capability at low (a) and high (b) current HPPC test of $LiFePO_4$/C-graphite battery.

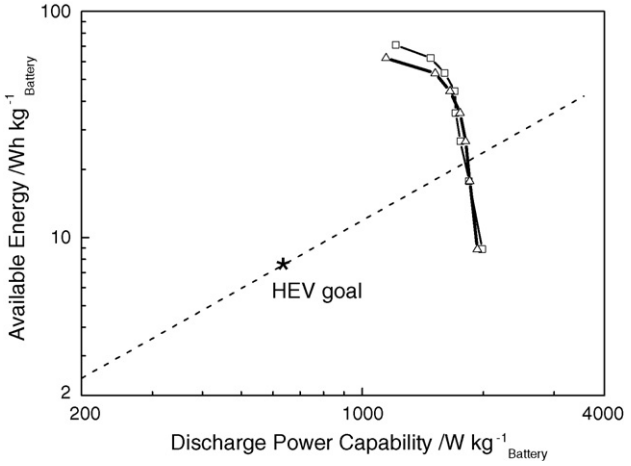

Fig. 10. Available specific energy *vs*. specific power capability of $LiFePO_4$/C-graphite battery from HPPC tests: (□) low-current, (△) high-current. The diagonal dashed line indicates the optimal P/E ratio for power-assist in HEV. The marker refers to the DOE goal.

only exception being the discharge pulse power at 90% DOD of the low-current HPPC test.

We took the lowest power capability plots *vs*. DOD, i.e. the P_{disc} plots from low- and high-current HPPC tests, and combined each with the plot of cumulative energy (E_{DOD}) *vs*. DOD from the SCT test to evaluate the available energy *vs*. pulse power capability of the battery. The results are shown in Fig. 10, a non-conventional Ragone plot which also reports the DOE goal for power-assist full HEV, and indicate that the $LiFePO_4$/C-graphite battery surpasses this goal.

4. Conclusions

$LiFePO_4$/C of high purity grade was successfully synthesized by MW accelerated sol–gel synthesis and showed excellent electrochemical performance in terms of specific capacity (up to 150 mAh g^{-1} at C-rate 0.1 C) and stability (confirmed up to 600 deep charge–discharge cycles at 1 C). This cathode material was also characterized in battery configuration with a graphite counter electrode by HPPC tests. It yielded a non-conventional Ragone plot that represents complexity of battery functioning in power-assist HEV and shows that the pulse power capability and available energy of such a battery surpasses the DOE goal for such an application. This is, to our knowledge, the first time that practical data (not simulated) of the dynamic functioning of this lithium-ion battery are reported.

$LiFePO_4$/C is also a suitable cathode material in power-assist HEV application because its flat operating potential and stable resistance over a wide DOD range keep its potential from lowering along the DOD range typical of other materials like $LiCoO_2$ and $LiMn_2O_4$. Moreover, the utilizable DOD range in the high-current HPPC test of the lithium-ion battery we tested was limited not by the cathode but by the anode, which lost capacity. Consequently, the use of an optimized graphite electrode may provide even better results for this battery.

Acknowledgement

Work funded by MIUR (Italy) PRIN 2007 Project “Lithium iron phosphate as cathode material for lithium-ion batteries for HEV and for charge storage from renewable intermittent sources”

References

[1] D. Jugović, D. Uskoković, J. Power Sources (2009), doi:10.1016/j.jpowsour.2009.01.074.
[2] M. Wohlfahrt-Mehrens, Chapter 17, Lithium Mobile Power 2007 October 29–30, San Diego CA, 2007.
[3] INEEL, FreedomCAR Battery Test Manual For Power-Assist Hybrid Electric Vehicles, Prepared for the U.S. Department of Energy (2003).
[4] S.G. Stewart, V. Srinivasan, J. Newman, J. Electrochem. Soc. 155 (9) (2008) A664.
[5] K. Chan, W. Town. Pharmaceutical-grade ferric organic compounds, uses thereof and methods of making same, World Intellectual Property Organization Patent No WO 2007/02/2435 (2007).
[6] C. Arbizzani, S. Beninati, L. Damen, M. Mastragostino, Solid State Ionics 178 (2007) 393–398.
[7] R. Dominko, et al., J. Electrochem. Soc. 152 (3) (2005) A607.
[8] I. Belharouack, C. Johnson, K. Amine, Electrochem. Comm. 7 (2005) 983.
[9] Y. Zhang, et al., Electrochim. Acta 54 (2009) 3206–3210.
[10] G.T. Kuo Fey, et al., J. Power Sources 189 (2009) 69–178.
[11] X.-F. Guo, et al., Solid State Ionics (2009), doi:10.1016/j.ssi.2008.11.021.